

Artifact-free Sound Quality in DNN-based Closed-loop Systems for Audio Processing

Chuan Wen, Guy Torfs, Sarah Verhulst, *Member, IEEE*

Abstract—Recent advances in deep neural networks (DNNs) have significantly improved various audio processing applications, including speech enhancement, synthesis, and hearing aid algorithms. DNN-based closed-loop systems have gained popularity in these applications due to their robust performance and ability to adapt to diverse conditions. Despite their effectiveness, current DNN-based closed-loop systems often suffer from sound quality degradation caused by artifacts introduced by suboptimal sampling methods. To address this challenge, we introduce dCoNNear, a novel DNN architecture designed for seamless integration into closed-loop frameworks. This architecture specifically aims to prevent the generation of spurious artifacts. We demonstrate the effectiveness of dCoNNear through a proof-of-principle example within a closed-loop framework that employs biophysically realistic models of auditory processing for both normal and hearing-impaired profiles to design personalized hearing aid algorithms. Our results show that dCoNNear not only accurately simulates all processing stages of existing non-DNN biophysical models but also eliminates audible artifacts, thereby enhancing the sound quality of the resulting hearing aid algorithms. This study presents a novel, artifact-free closed-loop framework that improves the sound quality of audio processing systems, offering a promising solution for high-fidelity applications in audio and hearing technologies.

Index Terms—deep learning, closed loop, audio processing, artifacts, sound quality.

I. INTRODUCTION

Recent advances in deep neural networks (DNN) have demonstrated remarkable success in various audio processing applications, such as speech synthesis [1]–[3], speech recognition [4], speech enhancement [5], hearing aid algorithms [6], and others. DNN-based closed-loop frameworks have become increasingly prevalent across various audio applications, primarily due to their notable performance improvements and high flexibility in adapting to diverse conditions. The generalized framework illustrated in Fig. 1 integrates an audio processor with a condition module that can be customized for different tasks. These include using generative adversarial networks (GAN) for audio synthesis [1]–[3], employing DNN-based loss functions for speech enhancement [7]–[10], and implementing biophysically inspired closed-loop frameworks for designing individualized hearing aid algorithms [6].

Chuan Wen and Sarah Verhulst are with the Hearing Technology Lab, Department of Information Technology, Ghent University, Ghent, Belgium. Guy Torfs is with IDLAB, Department of Information Technology, Ghent University, Ghent, Belgium.
E-mail: chuan.wen@ugent.be; guy.torfs@ugent.be; sarah.verhulst@ugent.be (Corresponding author: Chuan Wen)
This work was supported by FWO Machine Hearing 2.0 (216318G) and EIC-Transition EarDiTech (101058278).

However, current closed-loop frameworks are corrupted by the non-ideal downsampling and upsampling processes between the NN layers. The problematic operations can generate undesired artifacts, which degrade the resulting audio quality [11]. Specifically, typical downsampling methods, such as strided convolutions and average pooling, often lack low-pass filtering, leading to aliasing artifacts in low-frequency bands [3], [12]. Aliasing artifacts resulting from non-ideal downsampling methods degrade the harmonic components in the speech synthesis, leading to a noticeable decline in perceptual quality [13]. On the other hand, upsampling methods, such as transposed convolutions and pixel convolutions, tend to generate tonal artifacts that introduce noise in the high-frequency bands [3], [11]. Additionally, upsampling operations can produce imaging artifacts, where low frequencies are mirrored in high-frequency bands due to spectral replicas [3], [14]. For instance, [1] applied GANs to unsupervised audio generation. However, the use of transposed convolutions introduced pitched noise in the synthesized audio samples. Furthermore, [6] proposed a bio-inspired DNN-based closed-loop framework for designing hearing-aid (HA) algorithms. The autoencoder-based model (CoNNear) that is used within the closed-loop system comprises a differentiable description of the cochlea, inner-hair-cell (IHC), and auditory-nerve fiber (ANF) processing stages. However, the network produces audible artifacts that compromise the sound quality of the HA model. In these autoencoder-based auditory models (CoNNear_{cochlear}, CoNNear_{IHC} and CoNNear_{ANF}), the undesired artifacts originate from the transposed convolutions in the decoder.

To eliminate aliasing during upsampling and downsampling, Gaussian blur and low-pass filters can be used, as adopted in Alias-CNN [12] and stylegan3 [15], respectively. However, these methods resulted in reduced performance in speech synthesis tasks [14]. [14] modified the transposed convolution layer to blend high-frequency features from the input with low-pass filtered features at each upsampling stage. It showed potential in maintaining high performance while reducing aliasing artifacts. Alternative upsampling methods like linear interpolation have been proposed to eliminate the tonal artifacts [16], [17]. The linear interpolation can solve the problem of tonal artifacts, but still leaves imaging artifacts in the high-frequency bands [14].

We propose an artifact-free architecture (dCoNNear) designed to integrate the closed-loop systems for audio applications. We will illustrate the approach for hearing aid algorithms [6] with high sound quality. The dCoNNear is inspired by temporal convolutional networks (TCN) [18] and deep

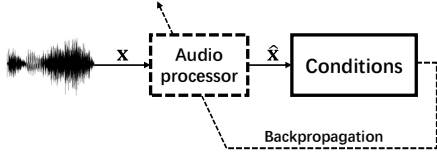


Fig. 1. Block diagram of the closed-loop framework for audio applications.

feedforward sequential memory networks (DFSMN) [19]. It comprises a sequence of stacked memory blocks. For each memory block, depthwise dilated 1-D convolutions are employed to model the long-term dependencies of auditory and audio processing (e.g. cochlear impulse response and neuronal adaptation) while avoiding the need for downsampling and upsampling in prior CoNNear-based systems. The dCoNNear architecture is applied to all auditory processing stages in the closed-loop system, including cochlear, IHC, and ANF, as well as the sound processor to train a hearing-aid signal processing algorithm (see Fig. 2). We show that dCoNNear accurately simulates all processing stages of non-DNN-based SOTA biophysical auditory processing without introducing spurious and audible artifacts in the resulting closed-loop trained audio application. We further extend the approach to a generalised artifact-free method for DNN-based closed-loop audio applications with high sound quality.

The rest of the paper is organized as follows: Section II provides an in-depth characterization of the artifacts. Section III introduces the proposed artifact-free dCoNNear-based closed-loop system. Section IV details the experimental procedures, while Section V outlines the evaluation methods. Sections VI and VII present the results and discussions, respectively. Finally, Section VIII concludes the study.

II. CHARACTERISTICS OF UPSAMPLING ARTIFACTS

The upsampling artifacts are well documented, [11] has demonstrated that transposed convolutions and subpixel convolutions introduce tonal artifacts, while nearest neighbor interpolation is prone to generating filtering artifacts. Additionally, during the upsampling process, the spectrum is cyclically repeated at the sampling rate, causing low-frequency components to be mirrored into high-frequency bands. This phenomenon leads to the replication of artifacts introduced by problematic upsampling methods, and the unintended presence of low-frequency components in high-frequency bands, commonly referred to as imaging artifacts. However, [11] analyzed only the artifacts after weight initialization, without providing a systematic analysis of the impact of the learning process on upsampling artifacts. In this section, we systematically characterize the artifacts generated by transposed convolutions, subpixel convolutions, and nearest neighbor interpolation when training the network for modeling auditory processing. We then studied artifacts associated with transposed convolution within the context of the closed-loop, CNN-based hearing aid algorithms [6].

To characterize the upsampling artifacts when employing neural networks to emulate the auditory model, we investigated

the artifacts of the autoencoder-based CoNNear_{cochlear} [20] with 4 encoders and decoders, herein referred to as prior CoNNear, between different upsampling methods. CoNNear_{cochlear} is a neural network representation of a non-linear transmission-line (TL) model that faithfully simulates the basilar-membrane (BM) displacement of human cochlear processing [21]. We examined three upsampling strategies in the decoders: transposed convolutions, subpixel convolutions, and nearest-neighbor interpolation. As depicted in Fig. 3, transposed and subpixel convolutions showed the peaks that were absent in the target model while the nearest-neighbor interpolation showed no obvious extra peaks in the step responses. To mitigate aliasing artifacts introduced by the strided convolution layers, which have a step size of 2, we applied a low-pass filter with a normalized cutoff frequency of 0.5 before each downsampling layer. All upsampling methods, however, showed additional spectral peaks in response to the 1-kHz tone. Previous studies have identified periodic tonal artifacts in transposed and subpixel convolutions due to problematic upsampling operators and spectral replicas after weight initialization [11]. In our findings, these artifacts persisted even after training. While nearest-neighbor interpolation is known to avoid tonal artifacts, it failed to effectively suppress imaging artifacts, resulting in noticeable peaks in the 1-kHz tone responses after training. These results suggest that the training process did not sufficiently resolve the artifacts caused by architectural limitations and spectral replicas, resulting in undesirable distortions in the model's output.

The artifacts associated with the autoencoder-based CoNNear models were systematically examined across each auditory processing stage depicted in Fig. 2, which include CoNNear_{cochlear}, CoNNear_{IHC} and CoNNear_{ANF} stages as part of the closed-loop system. These artifacts are identified and quantified using the deterministic auditory computational models [22], which served as targets during prior CoNNear training. Frequency responses for a 1-kHz tonal input across these stages are illustrated in Fig. 4(a-c). Fig. 4d shows the output of the HA model trained with the prior CoNNear framework to compensate for a high-frequency sloping hearing loss [6]. The prior CoNNear-based models exhibit spectral peaks in the magnitude spectrum of the cochlear, IHC, and ANF responses that are not present in the target model. During the training of the HA model, which minimizes the difference between NH and HI AN responses, the HA models incorporated tonal artifacts as shown in Fig. 4d. These artifacts degrade the resulting audio quality and should be systematically excluded from the closed-loop framework.

III. ARTIFACT-FREE DCONNEAR-BASED CLOSED-LOOP SYSTEM

The artifact-free dCoNNear-based closed-loop framework for individualized DNN-based hearing aid (HA) model training is illustrated in Fig. 2. This framework features two pathways: one for the AN response (r_f) of a normal hearing (NH) system, and the other for the response (\hat{r}_f) of a hearing-impaired (HI) system. Each pathway includes three primary components corresponding to distinct auditory processing stages, the cochlea,

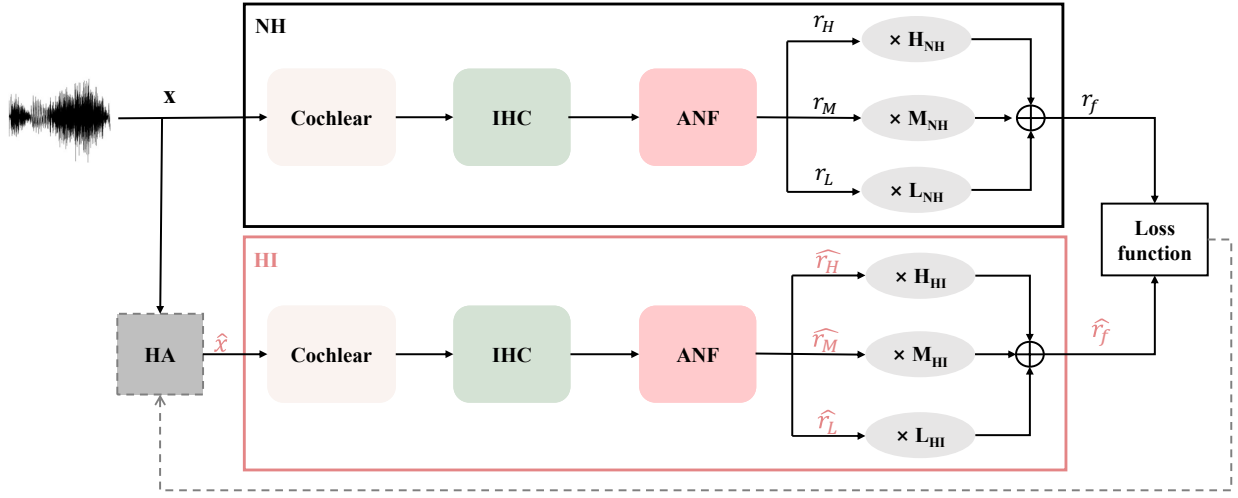


Fig. 2. Diagram of the closed-loop framework for designing individualized hearing aid algorithms.

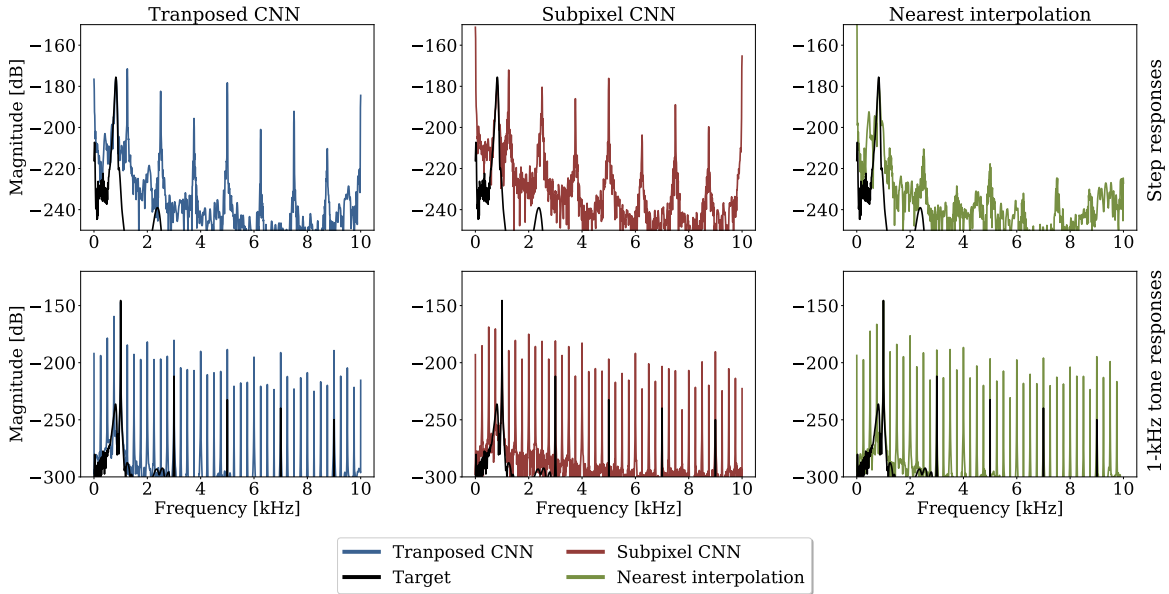


Fig. 3. Comparing the artifacts between different upsampling methods when training to simulate the TL model. The plots display the magnitude spectrum of BM displacement outputs at a center frequency of 1 kHz. From top to bottom, the stimuli consist of a step input and a 1 kHz pure tone at 70 dB SPL, respectively.

inner hair cells (IHC), and auditory nerve fibers (ANF). The NH AN response (r_f) is generated by combining three types of fibers (high-spontaneous rate (HSR), medium-spontaneous rate (MSR), and low-spontaneous rate (LSR)). These fibers are weighted by H_{NH} , M_{NH} , and L_{NH} , reflecting the typical innervation of each IHC in a healthy auditory system. To simulate hearing-impaired profiles, we adjust these weights to H_{HI} , M_{HI} , and L_{HI} to reflect the effects of cochlear synaptopathy (CS). The resulting AN responses (r_f) and (\hat{r}_f) provide biophysically realistic time-frequency representations of sound (neurograms), simulated at different cochlear locations. These neurograms reflect instantaneous firing rates across cochlear channels with center frequencies (CFs) ranging from 112 Hz to 12 kHz [23]. To tailor the hearing-impaired periphery to an individual's sensorineural hearing loss (SNHL)

profile, adjustments are made using audiometry to simulate the outer-hair-cell (OHC) damage in the cochlea or using auditory evoked potentials [24] to estimate CS. This involves introducing frequency-dependent OHC loss in $\text{CoNNear}_{\text{cochlear}}$ and/or CS in the $\text{CoNNear}_{\text{ANF}}$ model. The DNN-based HA models are subsequently trained by minimizing a predefined loss function between the simulated NH and HI responses [6]. All auditory elements and HA models within this framework are built upon the dCoNNear topology.

A. dCoNNear Architecture

Inspired by temporal convolutional networks (TCN) [25] and deep feedforward sequential memory networks (DFSMN) [19], we introduce the dCoNNear architecture, as shown in Fig. 5. The dCoNNear incorporates a series of stacked memory

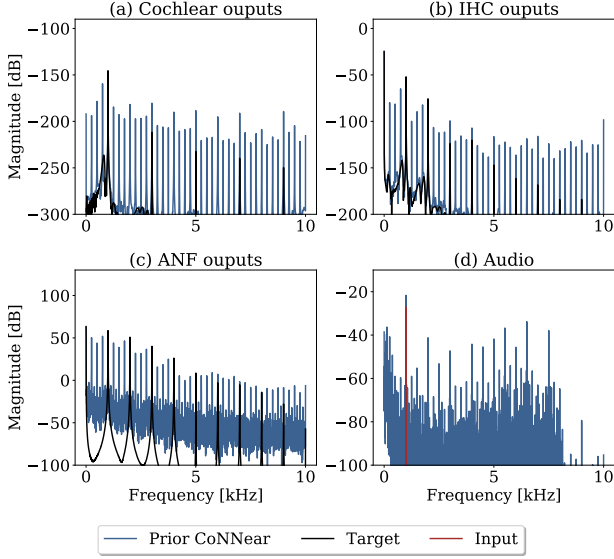


Fig. 4. The 1kHz tone response at different auditory processing stages compared against the target model for normal-hearing (a-c). (d) The 1-kHz tonal input against the output of the HA model trained from the CoNNear-based framework.

blocks that function similarly to a high-order finite impulse response (FIR) filter [19], enabling the network to capture extensive dependencies in sequential signals. The model employs M memory blocks with dilation factors 2^{m-1} , repeated R times, resulting in a total of $N = M * R$ blocks. Residual connections between memory blocks facilitate learning by addressing the vanishing gradient problem. Skip connections aggregate the outputs from each memory block through weighted summation, and these aggregated outputs are then processed by a non-linear activation function followed by a convolutional layer to produce the final model outputs [25].

The memory block (as shown in Fig. 5b) processes inputs from the previous block through pointwise convolution, followed by dilated depthwise convolution layers, D_h -conv and D_f -conv, which capture historical and future context information. Depthwise convolution applies a single filter per input channel, reducing the number of parameters and helping capture long-term dependencies while maintaining a compact model size. The outputs from the pointwise and depthwise convolution layers are combined, passed through an activation function, and directed to subsequent blocks and skip connection paths. The learnable FIR-like memory block [19] is formulated as:

$$\tilde{\mathbf{Y}}_t^\ell = \mathbf{Y}_t^\ell + \sum_{i=0}^{K_1^\ell} \mathbf{a}_i^\ell \odot \mathbf{Y}_{t-d_1 \cdot i}^\ell + \sum_{j=1}^{K_2^\ell} \mathbf{b}_j^\ell \odot \mathbf{Y}_{t+d_2 \cdot j}^\ell, \quad (1)$$

$$\mathbf{Y}_t^{\ell+1} = \mathbf{V}^\ell f(\tilde{\mathbf{Y}}_t^\ell) + \mathbf{U}^\ell \quad (2)$$

Here, $\mathbf{Y}_t^\ell = \mathbf{W}^\ell \mathbf{h}_t^\ell + \mathbf{B}^\ell$ represents the linear output of the ℓ -th projection layer. The parameters K_1^ℓ and K_2^ℓ define the look-back and lookahead orders, respectively, indicating the range of past and future data points considered. The dilation factors d_1 and d_2 help capture broader context information. The symbol \odot denotes element-wise multiplication, and $\mathbf{Y}_t^{\ell+1}$

is the output of the ℓ -th memory block at time t . The overall receptive field (RF) can be calculated as:

$$RF = K_1 + K_2 + R \sum_{i=0}^M (K_1 - 1) 2^i + R \sum_{j=0}^M (K_2 - 1) 2^j \quad (3)$$

Where K_1 and K_2 denote the kernel size of D_h -conv and D_f -conv respectively. This comprehensive approach ensures that the dCoNNear model effectively captures and processes long-term dependencies in audio and auditory signals, enhancing its performance for audio applications.

B. Auditory modules and HA model

Both normal hearing (NH) and hearing-impaired (HI) auditory peripheries, as shown in Fig. 2, utilize biophysically inspired CNN-based models that accurately simulate human cochlear, IHC and ANF processing: $dCoNNear_{\text{cochlear}}$, $dCoNNear_{\text{IHC}}$, and $dCoNNear_{\text{ANF}}$. The $dCoNNear_{\text{cochlear}}$ and $dCoNNear_{\text{IHC}}$ follow the dCoNNear topology, while $dCoNNear_{\text{ANF}}$ employs a three-branch structure to predict the different ANF types (HSR, MSR, and LSR).

When selecting hyperparameters, two primary considerations should be addressed: the receptive field (RF) and the specific activation function. A larger receptive field (RF) ensures that the CNN-based network accurately simulates the auditory model's impulse response. The selected activation functions need to capture the nonlinear characteristics of auditory processing, such as the compressive growth of the BM vibrations in the cochlear model and the rectification-like behavior of the IHCs. The framework's hyperparameters are detailed in Table I. Specifically, K_1 and K_2 denote the kernel sizes of the dilated depthwise convolution layers (D_h -conv and D_f -conv) within each memory block. The parameter H indicates the number of channels in the hidden layers. Additionally, L , L_l , and L_r represent the input length, left context, and right context, respectively.

The $dCoNNear_{\text{cochlear}}$ transforms acoustic signals into cochlear basilar-membrane vibrations. As described in [20], the hyperbolic tangent (Tanh) activation function was used, because it allows the activations to resemble the input-output relations of the auditory model and supports both positive and negative deflections of the basilar membrane.

The $dCoNNear_{\text{IHC}}$ model emulates the IHCs' function of sensing basilar membrane vibrations and converting them into IHC receptor potential changes. It employs a Tanh nonlinearity in the first stack and a sigmoid function in the second stack. This approach mirrors the compressive characteristics of the IHC input/output functions, with the sigmoid function effectively capturing the IHC receptor potential as a negative voltage difference [6].

The $dCoNNear_{\text{ANF}}$ model converts IHC receptor potentials into firing rates for three types of ANFs. The initial M blocks are shared layers, with each branch containing M blocks to independently generate HSR, MSR, and LSR fiber responses. The overall AN response (r_f) is derived by summing the three ANF responses. The ReLU activation function is applied here, as ANF processing differs from cochlear and IHC processing in that it only involves positive output values, without the

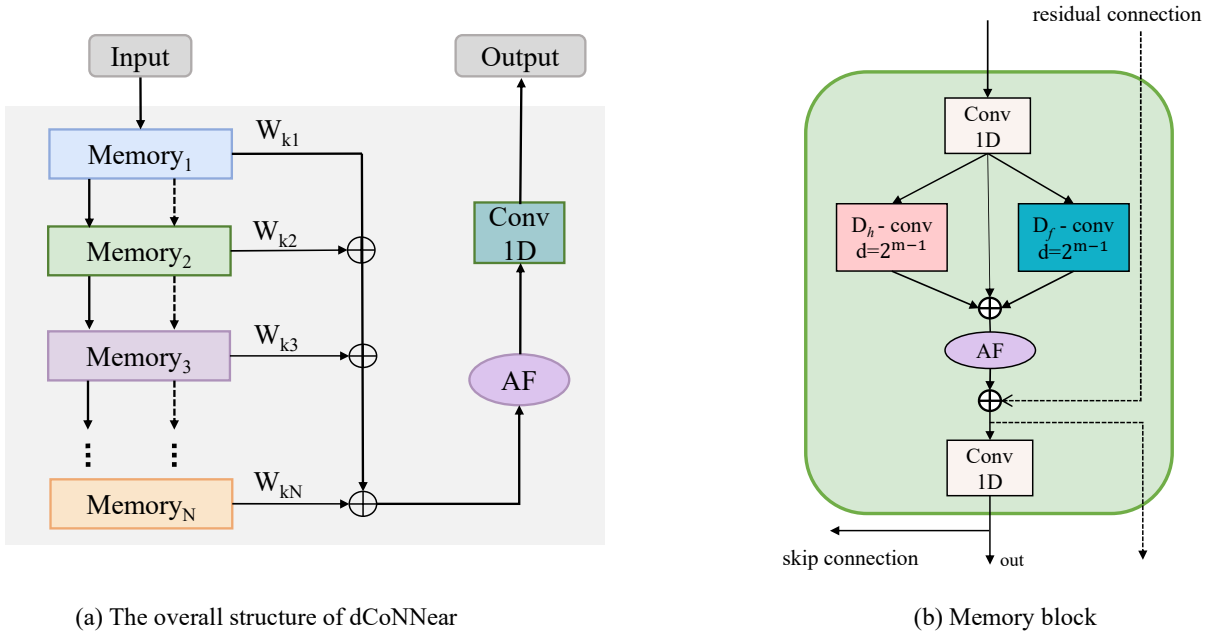


Fig. 5. (a) The block diagram of the dCoNNear. (b) The diagram of the memory block.

TABLE I

HYPERPARAMETERS OF THE dCoNNearS AND HA-MODEL. M AND R REPRESENT THE NUMBER OF MEMORY BLOCKS AND THE REPETITION NUMBER; K₁ AND K₂ DENOTE THE KERNEL SIZE OF D_h-CONV AND D_f-CONV IN EACH MEMORY BLOCK; H INDICATES THE CHANNEL NUMBER OF HIDDEN LAYERS; L, L_L, AND L_R REPRESENT THE INPUT LENGTH, LEFT CONTEXT, AND RIGHT CONTEXT, RESPECTIVELY

Models	M	R	K ₁	K ₂	H	Activation	Parameters	L _l	L _r
dCoNNear _{cochlear}	6	2	80	0	256	Tanh	1.5M	256	256
dCoNNear _{IHC}	4	2	32	32	128	Tanh	0.3M	256	256
dCoNNear _{ANF}	8	2	16	16	32	ReLU	0.1M	7936	256
HA-model	6	2	32	32	256	Tanh	1.6M	7936	256

compressive properties observed in the previous stages. The model features substantial left context windows of 7936 samples, ensuring accurate capture of the time-dependent recovery properties of the ANF models [26].

The DNN-based hearing-aid (HA) model is trained to restore NH AN responses. The Tanh nonlinearity is used to account for the compressive amplification characteristics of the human ear, similar to the wide-dynamic-range-compression (WDRC) strategy used in traditional hearing aids, which automatically adjusts amplification to amplify quiet sounds and compress loud sounds.

C. Individualisation of hearing impairment

To individualise hearing impaired pathway as shown in Fig. 2, we adjusted the normal hearing (NH) auditory modules to simulate different degrees of outer hair cell (OHC) loss and cochlear synaptopathy (CS) in the HI pathway. To simulate OHC loss, we retrained the NH cochlear model using transfer learning, based on a specific gain-loss profile or an individual audiogram [27]. The NH auditory nerve (AN) response (r_f) is computed as a weighted sum of the three ANF responses ($H_{NH} = 13$, $M_{NH} = 3$, and $L_{NH} = 3$). To simulate CS, the model was modified with adjusted weights H_{HI} , M_{HI} , and L_{HI} [6]. These personalized adjustments ensured the

models accurately represented individual hearing impairments, providing tailored audio processing solutions that minimized artifacts and preserved fidelity.

IV. TRAINING STRATEGY

The training procedure involved two main stages: (1) training the auditory modules (dCoNNear_{cochlear}, dCoNNear_{IHC}, and dCoNNear_{ANF}), and (2) training the HA model based on the closed-loop framework including the NH and HI pathways. Firstly, we trained the auditory modules using simulated responses from analytical models as targets, following the procedure outlined in [20], [26]. Once the auditory elements were trained, their parameters were frozen, and the HA models were then optimized within the closed-loop system as first described in [6].

A. Training auditory elements

The auditory module training targets were derived from various analytical models: a biophysical transmission line (TL) model for dCoNNear_{cochlear} [22], an analytical Hodgkin–Huxley-type model for dCoNNear_{IHC} [28], and a three-store diffusion model of the ANF synapse for dCoNNear_{ANF} [29]. To train these models, we used 2,310 utterances from the TIMIT speech corpus [30]. The input

signals were first upsampled to 100 kHz to accurately solve the reference models, and then downsampled to 20 kHz for training. The root-mean-square (RMS) energy of each sentence was adjusted to a specified sound pressure level (SPL) using the following equation:

$$signal = p_0 \cdot 10^{L_D/20} \cdot signal/RMS(signal) \quad (4)$$

where p_0 is the reference pressure of $2 \cdot 10^{-5}$ Pa, and L_D indicates the sound pressure level of the sound measured in decibels (dB).

1) *Training dCoNNear_{cochlear}*: The dCoNNear_{cochlear} model was trained to simulate basilar membrane (BM) displacements for 201 center frequencies between 112 Hz and 12 kHz [22], as human hearing sensitivity diminishes above 12 kHz. The RMS energy of each sentence was adjusted to $L_D = 70$ dB SPL. The input signal and TL-model outputs were segmented into windows of 2,048 samples, with left (L_l) and right (L_r) contexts of 256 samples each, resulting in a total input length of 2,560 samples. To facilitate training, a scaling factor of 10^6 was applied to the simulated BM displacements (expressed in [μm]), ensuring that the datasets maintained a statistical mean near zero and a standard deviation close to one.

2) *Training dCoNNear_{IHC} and dCoNNear_{ANF}*: The dCoNNear_{IHC} and dCoNNear_{ANF} were trained to simulate IHC potentials and ANF firing rates at 201 uniformly distributed center frequencies between 112 Hz and 12 kHz. The RMS energy of half the sentences was adjusted to 70 dB and 130 dB SPL, respectively, to cover a broad range of instantaneous intensities, enabling the models to capture the characteristic input-output and saturation properties of individual IHCs and ANFs.

For dCoNNear_{IHC}, the input signals were segmented into 2,048-sample windows with 256 context samples on both sides. For dCoNNear_{ANF}, the analytical IHC and ANF outputs were segmented into 8,192-sample windows, with 7,936 context samples before and 256 samples after each window. The simulated IHC potential outputs were multiplied by a factor of 10, expressed in [dV], and a scaling factor of 0.01 was applied to the simulated ANF outputs, expressed in [x100 spikes/s].

The training data for IHC and ANF, with dimension $N_{CF} = 201$, were converted into a one-dimensional dataset of $2,310 \cdot N_{CF}$ samples. This approach assumed that the reference IHC and ANF models had CF-independent parameters, while the BM displacements had CF-dependent impulse responses due to cochlear mechanics [26].

B. Training HA model

To train the HA model, the RMS energy of each utterance was adjusted to 70 dB SPL. The training dataset comprised 2,310 randomly selected utterances from the TIMIT corpus, segmented into windows of 8,192 samples. The inputs included 7,936 left context samples and 256 right context samples to meet the context window requirements of the dCoNNear_{ANF} model. The trained dCoNNear-based auditory models simulated cochlear responses at 201 center frequencies, ranging from 112 Hz to 12 kHz. For training the HA model, 21 equally spaced frequency channels were selected from the

201 to expedite the training process. During HA model optimization, the parameters of the dCoNNear auditory elements were kept frozen, and a predefined loss function was used to minimize the difference between the dCoNNear-simulated NH and HI AN responses.

C. Loss function

The training strategies from [20] and [26] were employed to train the dCoNNear_{cochlear}, dCoNNear_{IHC}, and dCoNNear_{ANF} models. The loss function for these models was optimized using the mean absolute error (MAE) between the analytical outputs and the predicted dCoNNear outputs.

For training the HA model parameters, we utilized a combined loss function that accounted for different representations of the differences between the NH responses r_f and the HI \hat{r}_f . As outlined in [6], additional constraints, such as population responses, were introduced to the training process to minimize features functionally relevant to hearing loss and auditory perception, given the highly nonlinear nature of auditory processing. The combined loss function incorporated both the AN responses and the AN population responses across all simulated CFs:

$$\ell_{HA} = \alpha \cdot \text{MSE}\{r_f(n, w), \hat{r}_f(n, w)\} + \beta \cdot \text{MSE}\{p(n), \hat{p}(n)\}, \quad (5)$$

$$p(n) = \sum_{w=1}^{N_{CF}} r(n, w), \quad (6)$$

$$\hat{p}(n) = \sum_{w=1}^{N_{CF}} \hat{r}(n, w) \quad (7)$$

where $\alpha = 30$ and $\beta = 1$ are the weights that balance the contributions of different losses during training. $p(n)$ and $\hat{p}(n)$ are the NH and HI AN population responses respectively, n corresponds to each sample of the AN population responses, and L to the total number of samples. This approach ensured that the model not only minimized the differences in the AN responses at each CF but also captured the overall population response across CFs, providing a more comprehensive and functionally relevant training strategy for the HA model.

D. Hearing impaired elements

We optimized the HA model to compensate for a specific hearing-impaired (HI) profile ‘‘Slope35-7,0,0’’ [6]. This profile represents a sloping high-frequency outer hair cell (OHC) loss beginning at 1 kHz, with hearing thresholds of 35 dB HL at 8 kHz, referred to as Slope35. Additionally, there is a complete loss of low spontaneous rate (LSR) and medium spontaneous rate (MSR) auditory nerve fibers (ANFs) ($H_{HI} = 0$ and $M_{HI} = 0$) and approximately 46% loss of high spontaneous rate (HSR) ANFs ($L_{HI} = 7$) to simulate the effects of age-related cochlear synaptopathy.

E. Training Setup

The learning rates for all model training was set to 10^{-4} . If the validation loss did not decrease over five consecutive epochs, the learning rate was halved to ensure optimal training

progression. All models were trained for 50 epochs using the Adam optimizer [31]. Training was conducted on three NVIDIA A30 GPUs using the PyTorch platform.

V. EVALUATION

To evaluate the artifact-free closed-loop system, we first examined whether the artifacts associated with the prior CoNNear architecture were eliminated and examined the sound quality of the resulting HA models. Additionally, we evaluated the biophysical properties of the dCoNNear auditory elements in comparison to the CoNNear architectures and the hearing loss restoration performance of the trained HA models.

A. Evaluating Artifacts

To determine whether the artifacts caused by the prior CoNNear were eliminated, we analyzed 70-dB SPL 1-kHz tone responses at various auditory processing stages, as well as the HA models trained within the closed-loop system based on both prior CoNNear and dCoNNear architectures. We quantified artifacts using total harmonic distortion (THD) at each step of the closed-loop system [32]. As aliased harmonics are generated by the prior CoNNear models in the 1-kHz tone responses as shown in Fig. 3, we examined harmonics at one-quarter intervals of the fundamental frequency:

$$\text{THD}_{\text{fractional}} = 20 \log_{10} \frac{\sqrt{\sum_{k=5}^{\infty} H_{k/4}^2}}{H_1} \quad (8)$$

where H_1 is the RMS value of the fundamental component, $H_{k/4}$ indicates the RMS of the fractional harmonics. A lower THD value indicates less harmonic distortion.

The Speech-to-Reverberation Modulation Energy Ratio (SRMR) [33] was used to evaluate the sound quality of the resulting HA models trained using both the prior CoNNear and dCoNNear-based frameworks. SRMR is a non-intrusive metric that assesses speech quality and intelligibility based on a modulation spectral representation of the speech signals. Higher SRMR scores indicate higher sound quality and fewer artifacts. We evaluated sound quality across three audio types: clean speech, noisy speech, and music. The clean speech dataset was 550 randomly selected utterances from TIMIT. The one-hour noisy speech dataset was generated by mixing the clean speech samples from TIMIT and the noise from Freesound [34] at SNR of 0 dB. The music dataset consisted of 100 randomly selected 30-second tracks from FMA [35].

B. Evaluating Auditory Elements

For each auditory model, we employed two evaluation metrics to assess whether the trained models accurately captured the relevant auditory properties.

For the dCoNNear_{cochlear}, we simulated the Q_{ERB} and basilar membrane (BM) excitation patterns, as described in [20]. The Q_{ERB} metric characterizes the level-dependent cochlear filter properties derived from the BM impulse response and is calculated as follows:

$$Q_{\text{ERB}} = \frac{\text{CF}}{\text{ERB}} \quad (9)$$

where equivalent-rectangular bandwidth (ERB) is determined from the power spectrum of a simulated BM time-domain response to an acoustic click stimulus with condensation clicks of $100\mu\text{s}$ duration at levels of 40 and 70 dB SPL. Cochlear excitation patterns reflect the nonlinear compressive growth of BM responses when the cochlea is stimulated with pure tones at CF corresponding to the cochlear measurement site. We calculated excitation patterns for 201 CF channels in response to pure tones at 0.5, 1, and 2 kHz frequencies, with levels ranging from 10 to 90 dB SPL.

For the dCoNNear_{IHC}, IHC excitation patterns and half-wave rectified IHC receptor potentials were measured. Similar to cochlear excitation patterns, IHC excitation patterns show a characteristic half-octave basal-ward shift of their maxima as stimulus level increases. We calculated excitation patterns for all 201 simulated IHC receptor potentials in response to pure tones of 0.5, 1, and 2 kHz frequencies and levels between 10 and 90 dB SPL. The half-wave rectified receptor potential demonstrates the compression feature of IHC mechanical-to-electrical transduction. To measure this, 4 kHz tonal stimuli with levels from 0 to 100 dB SPL were generated, and the IHC responses were then half-wave rectified by subtracting their DC component. The RMS of the rectified responses was computed for each level.

For the dCoNNear_{ANF}, rate-level curves and synchrony levels were measured [6]. Rate-level curves evaluate ANF responses to changes in stimulus level. We generated pure-tone stimuli (50-ms duration, 2.5-ms rise/fall ramp) with levels between 0 and 100 dB at frequencies of approximately 1 and 4 kHz, based on the corresponding CFs of the ANF models (1007 and 3972.7 Hz). The rate-level functions were derived by computing the average response 10–40 ms after stimulus onset. The ANF synchrony level describes the non-monotonic relation between ANF response and the stimulus level. Fully modulated 400-ms long pure tones with a modulation frequency f_m of 100 Hz and carrier frequencies of 3972.7 Hz (henceforth referred to as 4 kHz) were simulated, and the synchrony-level functions were calculated by extracting the magnitude of the f_m component from the Fourier spectrum of the fibers' firing rate.

C. Evaluating HA models

To evaluate the restoration performance of the trained HA models, we used normalized root-mean-square error (NRMSE) in [6], which was computed between the simulated NH and HI AN population responses, normalised to the maximum of the NH response for each sentence:

$$\text{NRMSE} = \frac{\text{RMSE}}{\max(p(n))}, \quad (10)$$

$$\text{RMSE} = \sqrt{\frac{1}{L} \sum_{n=1}^L (p(n) - \hat{p}(n))^2} \quad (11)$$

NRMSE calculations were performed on 550 randomly selected clean speech utterances from TIMIT, with RMS energy levels ranging from 40 to 70 dB SPL in 10 dB increments.

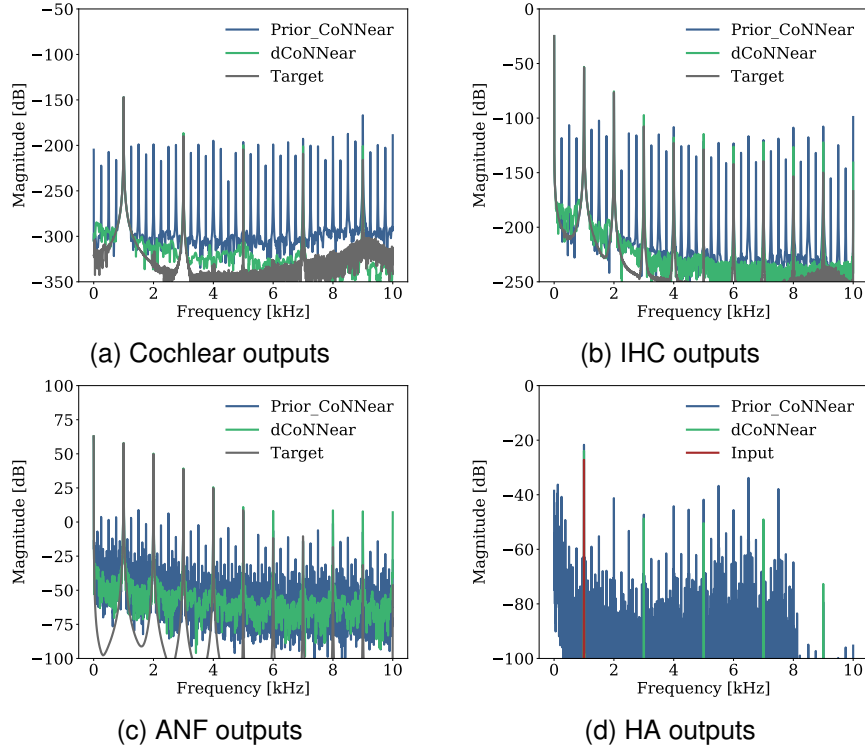


Fig. 6. The 1-kHz tone response at various auditory processing stages compared to the target models for normal hearing (a-c). (d) The 1-kHz tone responses of HA models trained using either the prior CoNNear or dCoNNear architecture. The target refers to simulations with non-DNN based auditory models that formed the basis for the DNN-based CoNNear model elements.

TABLE II
COMPARING THE THD ACROSS DIFFERENT MODELS FOR 1-KHZ PURE TONE RESPONSE

	Cochlear	IHC	ANF	HA
Analytical model	-54.65	-22.71	-8.05	-
Prior coNNear	-29.66	-20.47	-4.64	-28.06
dCoNNear	-32.92	-22.01	-8.16	-39.78

VI. RESULTS

In this section, we evaluated the proposed artifact-free dCoNNear-based closed-loop framework, designed for individualized DNN-based hearing aid (HA) models. The evaluation aimed to determine whether the artifacts associated with the prior CoNNear architecture were successfully eliminated in the dCoNNear-based auditory elements. We also compared the sound quality of the HA models trained with both the prior CoNNear and the new dCoNNear frameworks. Additionally, we assessed the biophysical properties of the auditory elements using stimuli that were not part of the training material. Finally, we compared the hearing aid restoration performance of the models developed using the prior CoNNear-based framework with those developed using the dCoNNear framework.

A. Artifacts and sound quality

Artifacts were examined using total harmonic distortion (THD) at each stage of auditory processing and the resulting HA models in both the prior CoNNear and dCoNNear models. The sound quality of the HA models was evaluated using the

non-intrusive metric SRMR on clean speech, noisy speech, and music samples.

Fig. 6 illustrates the 1-kHz tone responses at different auditory processing stages (panel a-c), as well as the HA models trained with diverse frameworks (panel d). The artifacts associated with the outputs of the dCoNNear models were markedly reduced compared to prior CoNNears, as observed by the difference between green and blue tonal lines in the magnitude spectrum. Table II shows the total harmonic distortions (THD) of the 1 kHz tone responses across different models. The THDs of the dCoNNear models decreased by 2 to 3.5 dB at each auditory processing stage compared to the prior CoNNear-based models, and the THD of the resulting HA outputs was reduced by 11.71 dB. This indicates that dCoNNear-based models effectively minimize the artifacts introduced by the prior CoNNear models, which enhances the resulting audio quality.

Table III compares the sound quality between prior CoNNear and dCoNNear for clean speech, noisy speech, and music, based on SRMR scores. For both clean and noisy speech, dCoNNear achieved higher SRMR scores than prior CoNNear, with the most significant improvement observed in noisy speech. This suggests that the dCoNNear-based model enhances the overall sound quality of the resulting speech signals. However, dCoNNear showed lower SRMR scores for music compared to prior CoNNear. This is likely due to the nature of music, which involves harmonics and overtones that are crucial for its perception. SRMR, however, primarily focuses on human vocal frequencies and modulations, and may not fully capture the complexities of music. Fig. 7

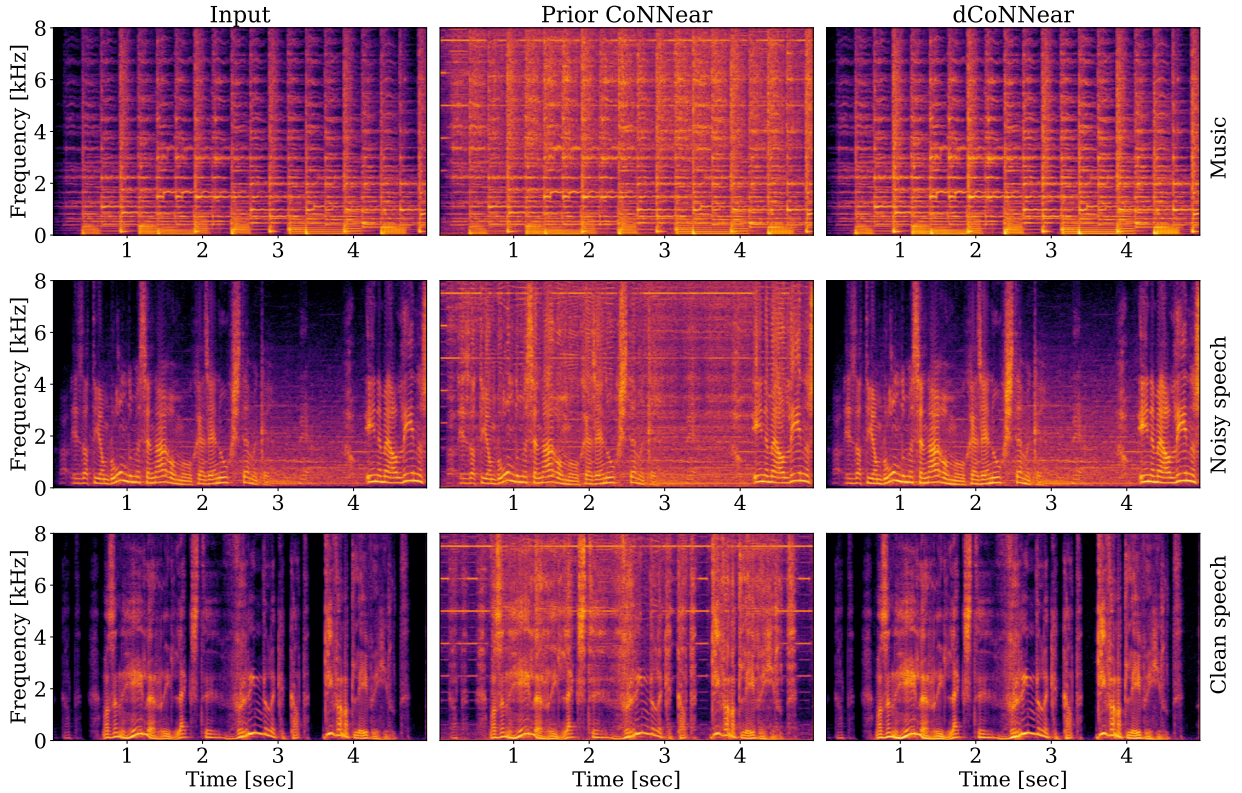


Fig. 7. Comparison of spectrograms processed by different HA models. The stimuli, from top to bottom, include music, clean speech, and noisy speech at 70 dB SPL.

TABLE III
COMPARISON OF SOUND QUALITY ACROSS DIFFERENT HA MODELS
BASED ON SRMR.

	Input	dCoNNear	prior CoNNear
Clean speech	7.39	6.77	6.13
Noisy speech	6.45	6.24	5.17
Music	1.93	1.75	1.91

displays example spectrograms for each audio type across the different models. The prior CoNNear models exhibited tonal artifacts (horizontal lines) for all audio types, which were not present in the original inputs. These artifacts were most noticeable in clean speech. In contrast, the horizontal lines were significantly reduced in the spectrograms of the dCoNNear models. Although the SRMR scores indicated that the sound quality of music was better for prior CoNNear than for dCoNNear, the spectrograms of music revealed that dCoNNear introduced far fewer artifacts compared to prior CoNNear. This suggests that dCoNNear effectively reduces artifacts across different audio types. The corresponding audio samples of music, clean speech, and noisy speech are provided at the link.

B. Biophysical properties of auditory modules

We employed auditory neuroscience techniques to quantify key properties of the dCoNNear-based auditory elements, comparing them against the reference analytical model and prior CoNNear outputs.

Figures 8 and 9 compare the basilar membrane (BM) excitation patterns and Q_{ERB} values of the proposed dCoNNear model with the reference TL model and prior CoNNear_{cochlear}. As shown in Fig. 8, dCoNNear exhibited performance comparable to both the prior CoNNear model and the TL model, suggesting that dCoNNear accurately captures the shape and compression properties of pure-tone cochlear excitation patterns. Fig. 9 illustrates a close match between dCoNNear, the reference TL model, and CoNNear_{cochlear}, indicating that dCoNNear reliably replicates the frequency-dependent characteristics of cochlear responses.

Figs. 10 and 11 present the IHC excitation patterns and the half-wave rectified IHC receptor potential, compared to the reference IHC model and prior CoNNear_{IHC} predictions. The excitation patterns from the dCoNNear_{IHC} model closely align with those of both the reference IHC model and prior CoNNear_{IHC} (Fig. 10). Fig. 11 shows the RMS of the half-wave rectified IHC receptor potential, V_{IHC} , in response to a 4-kHz pure tone across input levels ranging from 0 to 100 dB SPL. The blue curve, representing the dCoNNear_{IHC} model, follows the trends of the black and orange curves corresponding to the reference and prior models, respectively. This consistency indicates a nearly linear relationship with SPL up to 90 dB, followed by compressive growth beyond 90 dB SPL. These results suggest that the dCoNNear_{IHC} model accurately captures the potential-level growth characteristics.

Fig. 12(a) and (b) illustrate the ANF rate-level curves and synchrony levels, respectively, compared to the reference ANF model and prior CoNNear_{ANF} predictions. In Fig. 12(a),

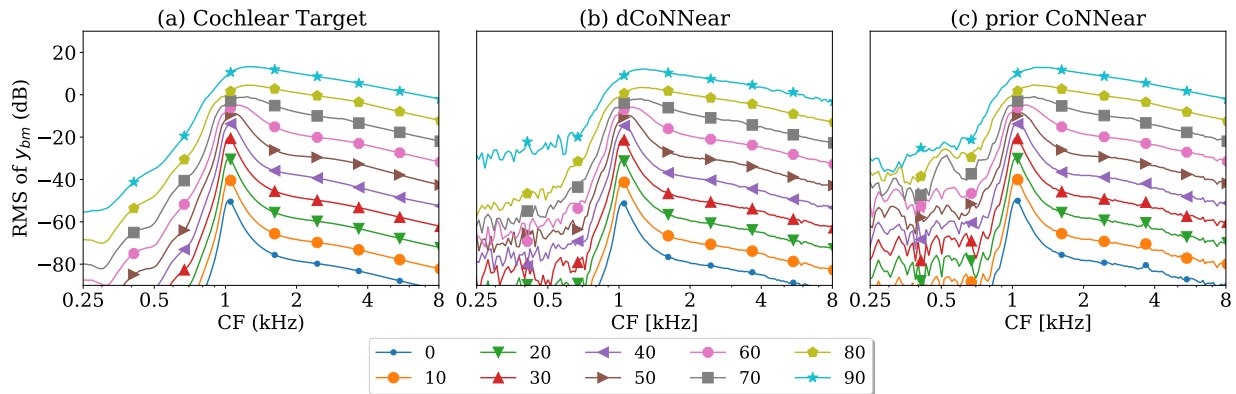


Fig. 8. Comparison of simulated RMS levels of basilar membrane (BM) displacement across center frequencies (CF) for pure-tone stimuli between 0 and 90 dB SPL with a step of 10 dB: (a) Target model, (b) dCoNNear model, (c) prior CoNNear model.

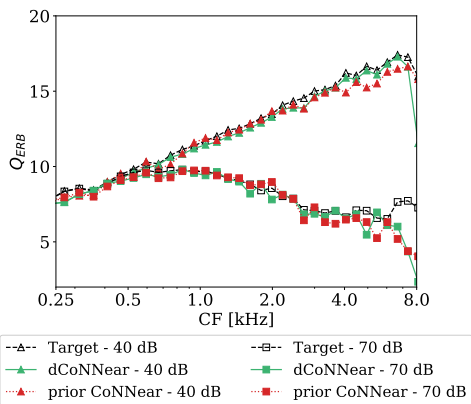


Fig. 9. Comparison of cochlear filter tuning (Q_{ERB}) across various center frequencies (CFs) using $100 \mu s$ clicks at 40 and 70 dB SPL among the dCoNNear model, the prior CoNNear model, and the target model.

the dCoNNear_{ANF} model showed consistent growth with the reference ANF model and prior CoNNear_{ANF} for HSR, MSR, and LSR types. This indicates that the dCoNNear_{ANF} model captures the level-dependent properties of different ANF types. Fig. 12(b) demonstrates that the dCoNNear_{ANF} model accurately represents the synchrony-level curves of the reference ANF model and prior CoNNear_{ANF} for all ANF types.

In conclusion, the dCoNNear-based auditory models faithfully replicate the auditory properties of the reference analytical models, ensuring accurate and reliable performance in auditory signal processing tasks.

C. Evaluation of restoration performance

The restoration performance of trained HA models based on different frameworks was evaluated and are presented in Table IV and Fig. 13.

Table IV presents the average normalized root-mean-square errors (NRMSEs) between the normal NH and HI AN population responses. These values were computed for the TIMIT utterances before and after processing with the HA models trained using the prior CoNNear and dCoNNear-based systems. To ensure a fair comparison, the same loss function was applied to train both HA models. Both models effectively reduced the NRMSEs of the AN population responses across different input levels, with more effective processing observed

TABLE IV
THE AVERAGE NRMSE PERCENTAGES ACROSS DIFFERENT HA MODELS FOR INPUT LEVELS BETWEEN 40 AND 70 dB SPL.

	40	50	60	70
Unprocessed	29.08	20.13	15.86	14.25
Prior CoNNear	20.13	15.41	14.67	13.12
dCoNNear	20.21	15.54	15.28	13.65

for speech presented at lower levels. However, the prior CoNNear exhibited marginally better performance than the dCoNNear. This may be attributed to the tonal artifacts generated by the HA models trained from the prior CoNNear-based system. As noted in [36], temporal peaks in sound can lead to increased AN responses, and high-frequency tonal artifacts can contribute to these elevated AN population responses.

To better understand how the processed audio affects the AN response features, Fig. 13 illustrates the time-domain speech segment along with the corresponding AN population responses before and after processing. A speech segment was processed by the two HA models and used as input to the HI auditory systems to simulate their AN population responses. The HA model trained using the prior CoNNear-based system introduced additional high-frequency fluctuations to the stimulus, enhancing the AN population responses but not fully restoring them. Conversely, the dCoNNear-based HA model introduced significantly fewer high-frequency fluctuations, resulting in a comparatively smaller increase in AN population responses. The additional high-frequency fluctuations stemmed from tonal artifacts introduced by the prior CoNNear, which increased AN population responses, but degraded the sound quality. This suggests that the tonal artifacts introduced by prior CoNNear contribute to restoring HI AN population responses, potentially enhancing hearing loss compensation. However, they compromised the sound quality of the resulting HA models. In conclusion, the dCoNNear-based models demonstrated comparable restoration performance while minimizing the artifacts introduced by prior CoNNear-based models, thereby achieving better overall sound quality.

VII. DISCUSSION

Current closed-loop frameworks suffer from non-ideal sampling processes, which can introduce undesired artifacts and

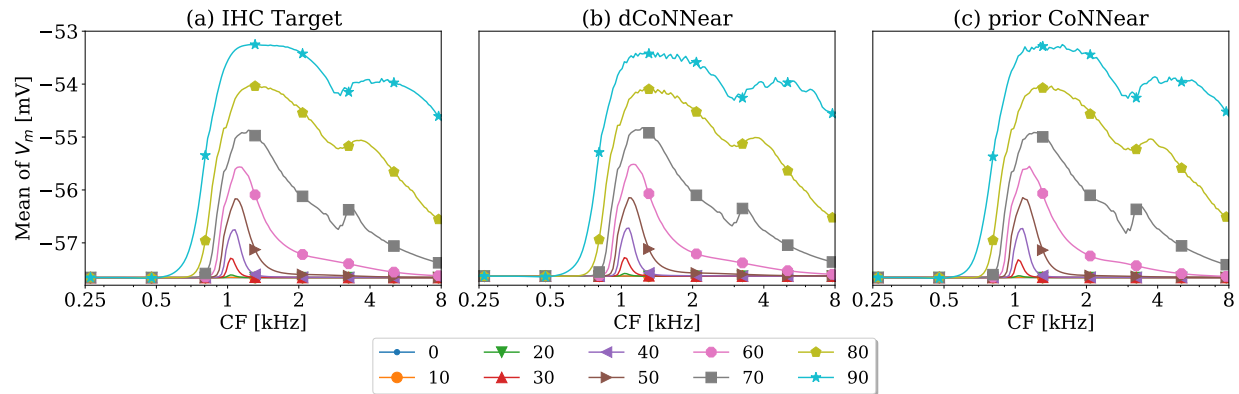


Fig. 10. Comparison of average IHC receptor potentials V_m across CFs for 1-kHz tone stimuli 0 to 90 dB SPL with a step of 10 dB: (a) target model, (b) dCoNNear model, and (c) prior CoNNear model.

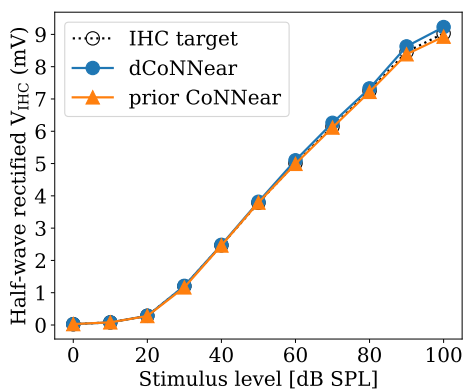


Fig. 11. Comparison of simulated dCoNNear_{IHC} half-wave rectified receptor potential in response to a 4-kHz pure tone across varying sound levels: (a) Target model, (b) dCoNNear model, (c) prior CoNNear model.

thus degrade the resulting audio quality. In this study, we systematically characterized the artifacts generated by different upsampling methods and examined those associated with transposed convolution within the context of closed-loop, autoencoder-based hearing aid algorithms. These artifacts originated from the interaction between problematic upsampling operations and spectral replicas by the upsampling layers. The artifacts persisted in the closed-loop system after training, leading to tonal artifacts in the resulting audio.

We propose an artifact-free architecture, dCoNNear, designed to integrate into closed-loop systems, exemplified here for hearing aid algorithms. In contrast to the existing autoencoder-based closed-loop system [6], the dCoNNear-based architecture can significantly reduce the artifacts associated with prior CoNNear models, thereby improving the sound quality of the resulting audio. This advancement provides an artifact-free framework for audio applications, delivering high sound quality for future audio processing algorithms.

While dCoNNear-based models successfully minimize artifacts associated with prior CoNNear, the SRMR scores of the processed samples decreased relative to the inputs, as shown in Table \ref{tab:SRMR}. One potential reason is the compressive amplification characteristics of the trained HA model, where quieter sounds are amplified more than

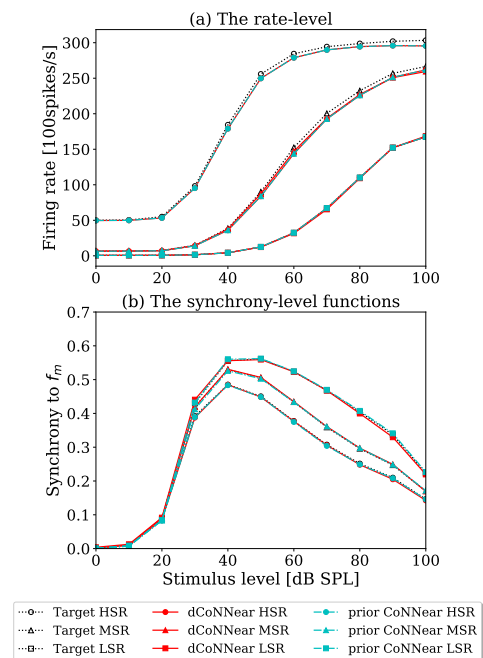


Fig. 12. Comparison of evaluation metrics for different emulated ANF models: Target, dCoNNear, and prior CoNNear. (a) ANF rate-level curves simulated for the HSR, MSR, and LSR ANF models at a CF of 4 kHz. (b) ANF synchrony-level functions for the HSR, MSR, and LSR ANF models at a CF of 4 kHz in response to a 4 kHz tone modulated by a 100 Hz tone.

louder sounds. This process amplifies low-level noise, which subsequently degrades sound quality. Therefore, incorporating a noise reduction module should be considered in future works. Another contributing factor could be the training process, which aimed to minimize differences between NH and HI auditory processing but may introduce non-linear distortions that affect sound quality. This study underscores the need for future research focused on developing more optimal loss functions or post-processing filters. Such developments would enhance the perceptual benefits of audio processing systems.

The current dCoNNear models are limited to wave-to-wave applications due to the absence of upsampling operations. This restricts their use to specific tasks such as speech enhancement, speech conversion, and hearing aids. Expanding the architec-

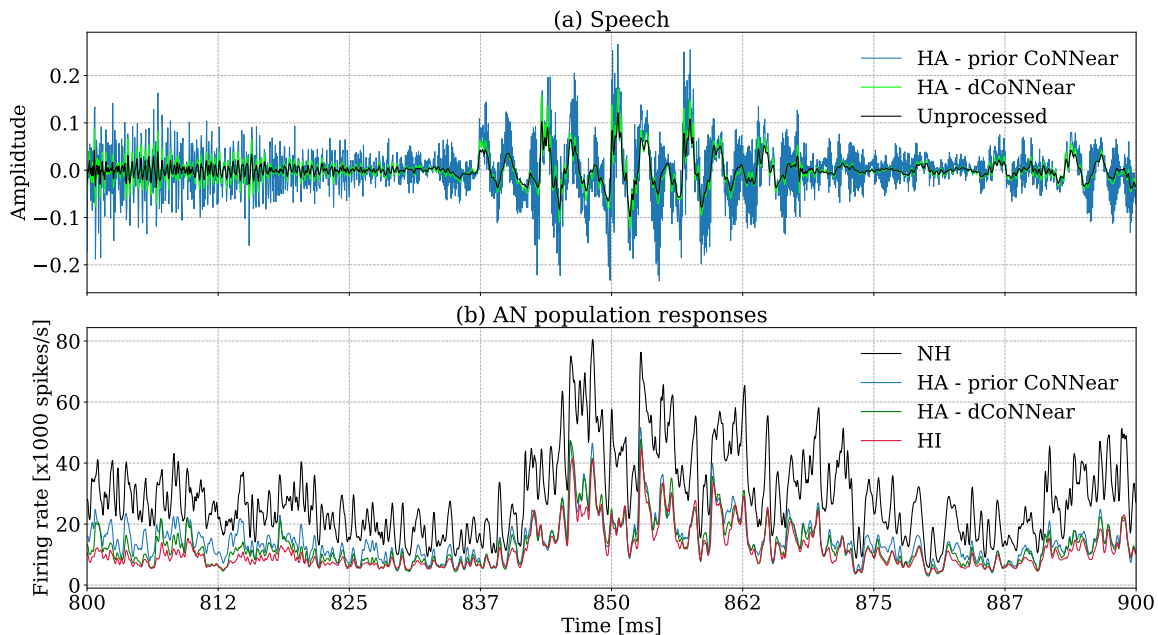


Fig. 13. Simulated auditory nerve (AN) population responses for hearing aid (HA) models trained using different frameworks at 70 dB SPL. (a) A clean speech segment is shown before and after processing with models trained using prior CoNNear (blue) and dCoNNear (green) systems. (b) The hearing-impaired (HI) AN population responses were enhanced after processing the input stimulus with different HA models. Ideal compensation would align the HI AN population responses with the NH AN population responses.

ture to include more versatile processing capabilities could broaden its applicability and effectiveness across various audio processing domains.

The use of the Speech-to-Reverberation Modulation Energy Ratio (SRMR) as an evaluation metric provided valuable insights into the sound quality of speech samples. However, SRMR falls short in evaluating other sounds types, such as music and environmental noises. This study suggests the need for broader objective metrics to assess a broader range of audio types. Additionally, while objective metrics are useful, subjective evaluations involving end-users are equally crucial. Incorporating user-centric evaluation metrics, such as the Hearing in Noise Test (HINT) [37] and Multiple Stimuli with Hidden Reference and Anchor (MUSHRA) [38], would provide a more comprehensive understanding of the perceptual benefits and real-world performance of DNN-based audio processing systems.

VIII. CONCLUSION

In this study, we systematically characterized the artifacts generated by different upsampling operations and examined those associated with transposed convolution within the context of closed-loop, autoencoder-based hearing aid algorithms. These artifacts stemmed from the interaction between problematic upsampling operations and spectral replicas created by the upsampling layers, compromising the sound quality of the resulting audio applications. To address these issues, we proposed an artifact-free architecture, dCoNNear, designed to integrate into closed-loop systems, specifically for hearing aid algorithms. The dCoNNear architecture incorporates a series of stacked FIR-like memory blocks, eliminating the need for sampling operations and demonstrating strong capability in

modeling long-term dependencies. Our results demonstrated that the dCoNNear-based models could significantly reduce the artifacts associated with autoencoder-based prior CoNNear models and improve the resulting audio quality. Additionally, dCoNNear not only accurately emulates all non-DNN-based biophysical auditory models but also shows comparable compensation performance to prior CoNNear models. The dCoNNear-based closed-loop framework holds great promise for advancing audio technologies, including hearing aids, speech enhancement, and speech conversion, with high sound quality.

REFERENCES

- [1] C. Donahue, J. McAuley, and M. Puckette, "Adversarial audio synthesis," in *International Conference on Learning Representations*, 2018.
- [2] J. Kong, J. Kim, and J. Bae, "Hifi-gan: Generative adversarial networks for efficient and high fidelity speech synthesis," *Advances in neural information processing systems*, vol. 33, pp. 17 022–17 033, 2020.
- [3] T. Bak, J. Lee, H. Bae, J. Yang, J.-S. Bae, and Y.-S. Joo, "Avocado: Generative adversarial network for artifact-free vocoder," in *Proceedings of the AAAI Conference on Artificial Intelligence*, vol. 37, no. 11, 2023, pp. 12 562–12 570.
- [4] O. Abdel-Hamid, A.-r. Mohamed, H. Jiang, L. Deng, G. Penn, and D. Yu, "Convolutional neural networks for speech recognition," *IEEE/ACM Transactions on audio, speech, and language processing*, vol. 22, no. 10, pp. 1533–1545, 2014.
- [5] S. R. Park and J. W. Lee, "A fully convolutional neural network for speech enhancement," *Evaluation*, vol. 10, p. 5, 2017.
- [6] F. Drakopoulos and S. Verhulst, "A neural-network framework for the design of individualised hearing-loss compensation," *IEEE/ACM Transactions on Audio, Speech, and Language Processing*, 2023.
- [7] F. Germain, Q. Chen, and V. Koltun, "Speech denoising with deep feature losses," in *Proceedings of the Annual Conference of the International Speech Communication Association, INTERSPEECH*, 2019.
- [8] S.-W. Fu, C.-F. Liao, and Y. Tsao, "Learning with learned loss function: Speech enhancement with quality-net to improve perceptual evaluation of speech quality," *IEEE Signal Processing Letters*, vol. 27, pp. 26–30, 2020.

- [9] Z. Xu, M. Strake, and T. Fingscheidt, “Deep noise suppression with non-intrusive pesqnet supervision enabling the use of real training data,” *arXiv preprint arXiv:2103.17088*, 2021.
- [10] S.-W. Fu, C. Yu, K.-H. Hung, M. Ravanelli, and Y. Tsao, “Metricgan-u: Unsupervised speech enhancement/dereverberation based only on noisy/reverberated speech,” in *ICASSP 2022-2022 IEEE International Conference on Acoustics, Speech and Signal Processing (ICASSP)*. IEEE, 2022, pp. 7412–7416.
- [11] J. Pons, S. Pascual, G. Cengarle, and J. Serrà, “Upsampling artifacts in neural audio synthesis,” in *ICASSP 2021-2021 IEEE International Conference on Acoustics, Speech and Signal Processing (ICASSP)*. IEEE, 2021, pp. 3005–3009.
- [12] R. Zhang, “Making convolutional networks shift-invariant again,” in *International conference on machine learning*. PMLR, 2019, pp. 7324–7334.
- [13] J. Zaidi, H. Seuté, B. van Niekerc12, and M.-A. Carbonneau, “Daft-exprt: Cross-speaker prosody transfer on any text for expressive speech synthesis,” 2022.
- [14] Z. Shang, H. Zhang, P. Zhang, L. Wang, and T. Li, “Analysis and solution to aliasing artifacts in neural waveform generation models,” *Applied Acoustics*, vol. 203, p. 109183, 2023.
- [15] T. Karras, M. Aittala, S. Laine, E. Härkönen, J. Hellsten, J. Lehtinen, and T. Aila, “Alias-free generative adversarial networks,” *Advances in neural information processing systems*, vol. 34, pp. 852–863, 2021.
- [16] A. Odena, V. Dumoulin, and C. Olah, “Deconvolution and checkerboard artifacts,” *Distill*, vol. 1, no. 10, p. e3, 2016.
- [17] D. Stoller, S. Ewert, and S. Dixon, “Wave-u-net: A multi-scale neural network for end-to-end audio source separation,” *arXiv preprint arXiv:1806.03185*, 2018.
- [18] C. Lea, R. Vidal, A. Reiter, and G. D. Hager, “Temporal convolutional networks: A unified approach to action segmentation,” in *Computer Vision—ECCV 2016 Workshops: Amsterdam, The Netherlands, October 8–10 and 15–16, 2016, Proceedings, Part III 14*. Springer, 2016, pp. 47–54.
- [19] S. Zhang, M. Lei, Z. Yan, and L. Dai, “Deep-fsmn for large vocabulary continuous speech recognition,” in *2018 IEEE International Conference on Acoustics, Speech and Signal Processing (ICASSP)*. IEEE, 2018, pp. 5869–5873.
- [20] D. Baby, A. Van Den Broucke, and S. Verhulst, “A convolutional neural-network model of human cochlear mechanics and filter tuning for real-time applications,” *Nature machine intelligence*, vol. 3, no. 2, pp. 134–143, 2021.
- [21] S. Verhulst, T. Dau, and C. A. SHERA, “Nonlinear time-domain cochlear model for transient stimulation and human otoacoustic emission,” *The Journal of the Acoustical Society of America*, vol. 132, no. 6, pp. 3842–3848, 2012.
- [22] S. Verhulst, A. Altoe, and V. Vasilkov, “Computational modeling of the human auditory periphery: Auditory-nerve responses, evoked potentials and hearing loss,” *Hearing research*, vol. 360, pp. 55–75, 2018.
- [23] D. D. Greenwood, “A cochlear frequency-position function for several species—29 years later,” *The Journal of the Acoustical Society of America*, vol. 87, no. 6, pp. 2592–2605, 1990.
- [24] S. Keshishzadeh, M. Garrett, and S. Verhulst, “Towards personalized auditory models: Predicting individual sensorineural hearing-loss profiles from recorded human auditory physiology,” *Trends in Hearing*, vol. 25, p. 2331216520988406, 2021.
- [25] Y. Luo and N. Mesgarani, “Conv-tasnet: Surpassing ideal time–frequency magnitude masking for speech separation,” *IEEE/ACM Transactions on Audio, Speech, and Language Processing*, vol. 27, no. 8, pp. 1256–1266, 2019.
- [26] F. Drakopoulos, D. Baby, and S. Verhulst, “A convolutional neural-network framework for modelling auditory sensory cells and synapses,” *Communications Biology*, vol. 4, no. 1, p. 827, 2021.
- [27] A. Van Den Broucke, D. Baby, and S. Verhulst, “Hearing-impaired bio-inspired cochlear models for real-time auditory applications,” in *21st Annual Conference of the International Speech Communication Association (INTERSPEECH 2020)*. International Speech Communication Association (ISCA), 2020, pp. 2842–2846.
- [28] A. Altoè, V. Pulkki, and S. Verhulst, “Model-based estimation of the frequency tuning of the inner-hair-cell stereocilia from neural tuning curves,” *The Journal of the Acoustical Society of America*, vol. 141, no. 6, pp. 4438–4451, 2017.
- [29] A. Altoe, V. Pulkki, and S. Verhulst, “The effects of the activation of the inner-hair-cell basolateral k⁺ channels on auditory nerve responses,” *Hearing research*, vol. 364, pp. 68–80, 2018.
- [30] J. S. Garofolo, L. F. Lamel, W. M. Fisher, J. G. Fiscus, and D. S. Pallett, “Darpa timit acoustic-phonetic continuous speech corpus cd-rom. nist speech disc 1-1.1,” *NASA STI/Recon technical report n*, vol. 93, p. 27403, 1993.
- [31] D. P. Kingma and J. Ba, “Adam: A method for stochastic optimization,” *arXiv preprint arXiv:1412.6980*, 2014.
- [32] D. Shmilovitz, “On the definition of total harmonic distortion and its effect on measurement interpretation,” *IEEE Transactions on Power Delivery*, vol. 20, no. 1, pp. 526–528, 2005.
- [33] T. H. Falk, C. Zheng, and W.-Y. Chan, “A non-intrusive quality and intelligibility measure of reverberant and dereverberated speech,” *IEEE Transactions on Audio, Speech, and Language Processing*, vol. 18, no. 7, pp. 1766–1774, 2010.
- [34] E. Fonseca, J. Pons Puig, X. Favory, F. Font Corbera, D. Bogdanov, A. Ferraro, S. Oramas, A. Porter, and X. Serra, “Freesound datasets: a platform for the creation of open audio datasets,” in *Hu X, Cunningham SJ, Turnbull D, Duan Z, editors. Proceedings of the 18th ISMIR Conference; 2017 oct 23–27; Suzhou, China.[Canada]: International Society for Music Information Retrieval; 2017. p. 486–93*. International Society for Music Information Retrieval (ISMIR), 2017. [Online]. Available: <https://arxiv.org/abs/1612.01840>
- [35] M. Defferrard, K. Benzi, P. Vandergheynst, and X. Bresson, “FMA: A dataset for music analysis,” in *18th International Society for Music Information Retrieval Conference (ISMIR)*, 2017. [Online]. Available: <https://arxiv.org/abs/1612.01840>
- [36] F. Drakopoulos, V. Vasilkov, A. O. Vecchi, T. Wartenberg, and S. Verhulst, “Model-based hearing-enhancement strategies for cochlear synaptopathy pathologies,” *Hearing Research*, vol. 424, p. 108569, 2022.
- [37] J. B. Nielsen and T. Dau, “The danish hearing in noise test,” *International journal of audiology*, vol. 50, no. 3, pp. 202–208, 2011.
- [38] B. Series, “Method for the subjective assessment of intermediate quality level of audio systems,” *International Telecommunication Union Radio-communication Assembly*, vol. 2, 2014.